CRYSTAL
GROWTH
& DESIGN
2008
VOL. 8, NO. 4
1161–1172

Supramolecular Approach to the Synthesis of [60]Fullerene−Metal Dithiocarbamate Complexes, $\{(M^{II}(R_2dtc)_2)_x \cdot L\} \cdot C_{60}$ (M = Zn, Cd, Hg, Fe, and Mn; $x = 1$ and 2). The Study of Magnetic Properties and Photoconductivity

Dmitri V. Konarev,[*,†] Salavat S. Khasanov,[‡] Andrey Yu. Kovalevsky,[§] Dmitri V. Lopatin,[⊥]
Vyacheslav V. Rodaev,[⊥] Gunzi Saito,[¶] Bálint Náfrádi,[#] László Forró,[#] and
Rimma N. Lyubovskaya[*,†]

Institute of Problems of Chemical Physics RAS and Institute of Solid State Physics RAS, Chernogolovka, Moscow Region 142432, Russia, State University of New York at Buffalo, Buffalo, New York, 14260, Department of Physics, Tambov State University, Tambov, 392622 Russia, Division of Chemistry, Graduate School of Science, Kyoto University, Kyoto 606-8502, Japan, and Institute of Physics of Complex Matter, EPFL, Lausannne CH-1015, Switzerland

Received March 13, 2007; Revised Manuscript Received October 12, 2007

ABSTRACT: Coordination assemblies formed by metal(II) dithiocarbamates $M^{II}(R_2dtc)_2$ (M = Zn, Cd, Hg, Mn, and Fe; R = Me, Et, *i*Pr, *n*Pr, and *n*Bu) and nitrogen-containing ligands (L = DABCO, DMP, and HMTA) are shown to be sterically well consistent with the spherical shape of fullerenes and are effectively cocrystallized with them to form complexes $\{(M^{II}(R_2dtc)_2)_x \cdot L\} \cdot C_{60}$ ($x =$ 1 and 2) with layered or three-dimensional (3D) packing of fullerene molecules (**1**−**11**). For the first time the molecular structures of the $M^{II}(R_2dtc)_2$ assemblies in the complexes with C_{60} are presented (including those with M = Mn, Fe, and Hg). According to optical and electron paramagnetic resonance (EPR) spectroscopy **1**−**11** have a neutral ground state. Magnetic susceptibilities of $\{[M^{II}(Et_2dtc)_2]_2 \cdot DABCO\} \cdot C_{60} \cdot (DABCO)_2$ (M = Mn and Fe) follow the Curie–Weiss law in the 50–300 K range with the Weiss constants $\Theta = 0.35$ and 1.70 K, respectively. Magnetic moments of the complexes equal to 8.23 and 6.88 μ_B at 300 K correspond to the high-spin state of the Mn^{II} ($S = 5/2$) and Fe^{II} ($S = 2$) ions. The increase of μ_{eff} observed below 35 and 50 K up to 8.5 μ_B (at 3 K) and 7.4 μ_B (at 6 K) indicates the manifestation of short-range ferromagnetic interactions between M^{II} spins in the isolated $[M^{II}(Et_2dtc)_2]_2 \cdot DABCO$ dimers. Under illumination by white light, the complexes show up to 10^2 times increase of photocurrent. The main contribution to the generation of free charge carriers is provided by direct charge transfer from $\{M^{II}(R_2dtc)_2\}_2 \cdot L$ to C_{60}. It was found that photocurrent increases in magnetic field with induction $B < 1$ T.

Introduction

Donor–acceptor complexes based on fullerenes are now intensively studied due to their promising magnetic and optical properties.[1] Donor molecules of different types were used to be cocrystallized with fullerenes. Those are calixarenes,[2] aromatic hydrocarbons,[3] substituted tetrathiafulvalenes,[4] amines,[5] metal octaethyl- and tetraphenylporphyrins,[6] metal dithiocarbamates,[7] and some other compounds.[1,4c] To effectively cocrystallize with fullerene spheres, donor molecules should have either flexible ethyl or phenyl substituents as metal octaethyl- and tetraphenylporphyrins,[6] concave or butterfly-like shape of the molecules as calixarenes,[2] cyclotriveratrylene,[8] dianthracene,[3a] and some metal dithiocarbamates.[7a,b] All of the above-mentioned complexes are neutral ones and usually contain only one donor component ($D \cdot C_{60}$) or in some cases involve solvent molecules ($D \cdot C_{60} \cdot Sol.$) as well. The modification of fullerene complexes through the incorporation of a third component allows one to affect their crystal structures and in some cases the charged state of donor or fullerene molecules and, consequently, the physical properties of the complexes. Molecules with strong donor or acceptor properties,[9] *N*-containing ligands,[10] or cations[11] can be incorporated into the $D{-}C_{60}$ framework. The two latter approaches can be classified as supramolecular ones since they use relatively weak coordination bonding between metal-containing donors (D) and *N*-containing ligands (L) or cations (C^+) to incorporate them into the complex with the formation of neutral $(D \cdot L) \cdot C_{60}$ or ionic $(D \cdot C^+) \cdot (C_{60}^-)$ multicomponent complexes.

Scheme 1

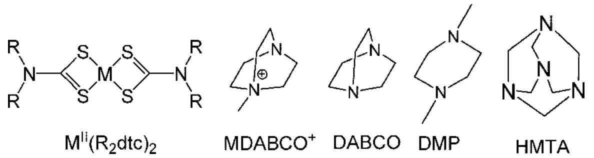

Metalloporphyrins demonstrate high synthetic potential in these approaches. For example, molecular complexes of C_{60} with zinc tetraphenylporphyrin (D = ZnTPP) monomers, dimers, and pentamers bonded by pyridine, tetramethylethylenediamine, pyrazine, 4,4′-bipyridine, and tetrapyridylporphyrin as L were obtained and structurally characterized.[10] *N*-containing coordinating methyldiazabicyclooctane (C^+ = $MDABCO^+$, Scheme 1) cation forms a series of ionic complexes: $\{(MDABCO^+)_n \cdot M^{II}porphyrin)\} \cdot (C_{60}^-)_n$ ($n = 1$ and 2), where porphyrin can be octaethylporphyrin (OEP), tetrakis(4-methoxyphenyl)porphyrin (TMPP), and tetraphenylporphyrin (TPP), and M is Co, Zn, Fe, and Mn).[11] In these complexes, we observed the reversible formation of the $Co{-}C(C_{60}^-)$ coordination bonds with the paramagnetic−diamagnetic transition in $\{(MDABCO^+) \cdot Co^{II}OEP \cdot (C_{60}^-)\} \cdot (C_6H_5CN)_{0.67} \cdot (C_6H_4Cl_2)_{0.33}$,[11a] a new $(C_{60}^-)_2$ dimer bonded by two single bonds in $\{(MDABCO^+) \cdot$

---

[*] Corresponding authors. Tel./Fax: +007-496-522-1852. E-mail: konarev@icp.ac.ru (D.V.K.); lyurn@icp.ac.ru (R.N.L.).
[†] Institute of Problems of Chemical Physics RAS.
[‡] Institute of Solid State Physics RAS.
[§] State University of New York at Buffalo.
[⊥] Department of Physics, Tambov State University.
[¶] Division of Chemistry, Graduate School of Science, Kyoto University.
[#] Institute of Physics of Complex Matter.

10.1021/cg0702481 CCC: $40.75

$Co^{II}TMPP\}_2\cdot(C_{60}^{-})_2\cdot(C_6H_4Cl_2)_{2.5}\cdot(C_6H_5CN)_{1.5}$,[11b] and antiferromagnetically coupled $C_{60}^{\bullet-}$ chains or diamagnetic $(C_{70}^{-})_2$ dimers in $\{(MDABCO^+)_2\cdot M^{II}TPP\}\cdot(C_{60(70)}^{-})_2\cdot(C_6H_4Cl_2)_{2.2+x}\cdot(C_6H_5CN)_y$ (M = Zn, Co, Mn, and Fe, $x = 0 - 2.2$, $y = 0 - 1.8$).[11c]

Metal(II) dithiocarbamates present another wide family of organometallic donors (Scheme 1), which can also be promising components in the design of photoactive and magnetic complexes with fullerenes having neutral and ionic ground states.[7] For example, layered C_{60} and C_{70} complexes with Cu^{II} and Cd^{II} diethyldithiocarbamates manifest photoconductivity, whereas the C_{70} complex with Mn^{II} diethyldithiocarbamate shows strong antiferromagnetic coupling.[7b] The reversible dimerization of $C_{60}^{\bullet-}$ is observed in ionic $(Cr^{I}(C_6H_6)_2^{\bullet+})\cdot[Pd(dbdtc)_2]_{0.5}\cdot(C_{60}^{\bullet-})$ ($Cr(C_6H_6)_2$: bis(benzene)chromium); $Pd(dbdtc)_2$: Pd^{II} dibenzyldithiocarbamate).[7c] Similarly to metalloporphyrins, metal(II) dithiocarbamates are able to form various coordination assemblies, which, however, were studied only for zinc and cadmium dialkyldithiocarbamates,[12] and one coordination dimer with tellurium(II) dithiocarbamate is known[13] (according to CCDC data). Dimers were formed with 4,4′-bipyridine, bis(4-pyridyl)ethylene, tetramethylethylenediamine,[12a−c,13] whereas pyridine, imidazole, 2,2′-bipyridine, phenanthroline, and trimethylphosphine were used to obtain coordination monomers with metal(II) dithiocarbamates.[12d−g]

In this work, we for the first time applied a supramolecular approach to incorporate N-containing ligands into metal(II) dithiocarbamate−fullerene complexes to modify their crystal structures and affect their physical properties. New coordination assemblies of metal dithiocarbamates with bidentant diazabicyclooctane (DABCO), *N,N*′-dimethylpiperazine (DMP) and tetradentant hexamethylenetetramine (HMTA) were obtained (Scheme 1). In addition to Zn and Cd dithiocarbamates, coordination assemblies with Mn^{II}, Fe^{II}, and Hg^{II} dithiocarbamates were prepared. These assemblies effectively cocrystallized with C_{60} to form complexes **1**–**11**. The crystal structures of eight complexes were solved. The complexes were characterized by IR- and UV–visible−NIR spectra. Temperature-dependent SQUID and electron paramagnetic resonance (EPR) measurements were performed for the complexes containing coordination dimers of paramagnetic Mn^{II} and Fe^{II} diethyldithiocarbamates. Photoconductivity was measured on single crystals of $[\{Zn(Et_2dtc)_2\}_2\cdot DABCO]\cdot C_{60}\cdot(DABCO)_2$ (**4**), $[\{Cd(nPr_2dtc)_2\}_2\cdot DMP]\cdot(C_{60})_5\cdot(C_6H_5Cl)_4$ (**8**), and $[\{Hg(nPr_2dtc)_2\}_2\cdot DMP]\cdot(C_{60})_5\cdot(C_6H_5Cl)_4$ (**9**). The comparative analysis of photoconductivity and absorption spectra allows the mechanisms of free charge carrier generation in these complexes to be elucidated. The effect of a weak magnetic field on photocurrent was studied.

Experimental Section

Materials. Sodium diethyldithiocarbamate trihydrate ($Na(Et_2dtc)\cdot 3H_2O$), diazabicyclooctane (DABCO), *N,N*′-dimethylpiperazine (DMP), and hexamethylenetetramine (HMTA) were purchased from Aldrich, and $Zn(nBu_2dtc)_2$ was purchased from Wako. Sodium ethylmethyldithiocarbamate [Na(EtMedtc)], sodium di(*i*-propyl)dithiocarbamate [$Na(iPr_2dtc)$], and sodium di(*n*-propyl)dithiocarbamate [$Na(nPr_2dtc)$] were obtained and recrystallized by the reported procedure.[14,7b] $M(Et_2dtc)_2$ (M = Zn, Cd, Fe^{II}, and Mn^{II}) were obtained according to the previously described method.[7b] C_{60} of 99.98% purity was used from MTR Ltd. $C_6H_4Cl_2$ and C_6H_5Cl over CaH_2, hexane over Na/benzophenone were distilled in argon atmosphere. For the synthesis of air-sensitive $M(Et_2dtc)_2$ (M = Fe^{II} and Mn^{II}) and the preparation of their fullerene complexes, solvents were degassed and stored in a MBraun 150B-G glovebox with controlled atmosphere and the content of H_2O and O_2 less than 1 ppm. The crystals of **5** and **6** were stored in a glovebox and were sealed in 2 mm quartz tubes for EPR and SQUID measurements under 10^{-5} Torr. KBr pellets for IR- and UV–visible−NIR measurements were prepared in a glovebox.

Synthesis. For the preparation of $[\{Cd(EtMedtc)_2\}_2\cdot DABCO]\cdot C_{60}\cdot(C_6H_5Cl)_{0.5}$ (**1**), $\{Cd(EtMedtc)_2\}_2\cdot DABCO$ was generated in situ without isolation. $CdBr_2\cdot 4H_2O$ (30 mg, 0.087 mmol), two molar equivalents of Na(EtMedtc) (27 mg, 0.174 mmol), and an excess of DABCO (100 mg, 0.9 mmol) were stirred in chlorobenzene solution (15 mL) for 4 h at 60 °C. The solution was cooled down and filtered, and C_{60} (25 mg, 0.035 mmol) was dissolved for 2 h at 60 °C. The solution was cooled down again and filtered, and 1 mL of benzonitrile was added to prevent the precipitation of the excess of DABCO and $\{Cd(EtMedtc)_2\}_2\cdot DABCO$ at the end of the evaporation. Evaporation of solution during one week gave the crystals of **1**. The crystals were filtered off and washed with several portions of acetone to afford black elongated parallelepipeds of **1** with 60% yield.

The crystals of $[\{Zn(Et_2dtc)_2\}_2\cdot DABCO]\cdot C_{60}\cdot C_6H_5Cl$ (**2**) were obtained by evaporation. C_{60} (25 mg, 0.035 mmol), $Zn(Et_2dtc)_2$ (29 mg, 0.07 mmol), and an excess of DABCO (100 mg, 0.9 mmol) were dissolved in 16 mL of chlorobenzene/benzonitrile solution (15:1) by stirring for 2 h at 60°. Evaporation of chlorobenzene during one week afforded the crystals of **2**. The crystals were filtered off and washed with several portions of acetone to give black parallelepipeds of **2** with 70% yield.

High-quality crystals of $[\{M(Et_2dtc)_2\}_2\cdot DABCO]\cdot C_{60}\cdot(DABCO)_2$(M = Zn, Cd, Mn^{II}, and Fe^{II}; **3**–**6**) and $[\{Cd(iPr_2dtc)_2\}_2\cdot DABCO]\cdot C_{60}\cdot(C_6H_{14})_{0.88}\cdot(C_6H_4Cl_2)_{0.12}$ (**7**) were obtained by diffusion. $M(Et_2dtc)_2$ (42–48 mg, 0.105 mmol)(**3**–**6**) or $Cd(iPr_2dtc)_2$ (**7**) (53 mg, 0.105 mmol), C_{60} (25 mg, 0.035 mmol), and an excess of DABCO (100 mg, 0.9 mmol) were dissolved in dichlorobenzene (12 mL) for 4 h at 60 °C. The solution was cooled down and filtered to the tube for the diffusion of 45 mL volume, and 30 mL of hexane was layered over the dichlorobenzene solution. After one month, large prisms grew on the walls of the tubes in a hexane part of the solution.

For the preparation of $[\{M(nPr_2dtc)_2\}_2\cdot DMP]\cdot(C_{60})_5\cdot(C_6H_5Cl)_4$ (M = Cd, and Hg, **8**, **9**), $\{M(nPr_2dtc)_2\}_2\cdot DMP$ was generated in situ without isolation. $CdBr_2\cdot 4H_2O$ or $Hg(CH_3COO)_2\cdot 4H_2O$ (0.087 mmol), two molar equivalents of $Na(nPr_2dtc)$ (34.6 mg, 0.174 mmol), and an excess of DMP (1 mL) were stirred in chlorobenzene solution (15 mL) for 4 h at 60 °C. The solution was cooled down and filtered, and C_{60} (25 mg, 0.035 mmol) was dissolved for 2 h at 60 °C. The resulting solution was cooled down again and filtered. Evaporation of the solution during one week afforded the crystals of **8** and **9**. The crystals were filtered off and washed with several portions of acetone to give black large prisms (up to 2 × 1 × 0.5 mm) of **8** and **9** with 60–80% yield. X-ray analysis showed complex **8** to be isostructural to **9**.

$[\{Zn(nBu_2dtc)_2\}_2\cdot DMP]\cdot(C_{60})_7\cdot(C_6H_5Cl)_4$ (**10**) was obtained by the evaporation of 15 mL of chlorobenzene solution containing C_{60} (25 mg, 0.035 mmol), $Zn(nBu_2dtc)_2$ (50 mg, 0.105 mmol), and an excess of DMP (1.2 mL). Evaporation of chlorobenzene during one week afforded the crystals of **10**. The crystals were filtered off and washed with several portions of acetone to afford black elongated plates with 80% yield.

For the preparation of $[\{Zn(Et_2dtc)_2\}\cdot HMTA]_2\cdot C_{60}\cdot C_6H_5Cl$ (**11**), C_{60} (25 mg, 0.035 mmol), $Zn(Et_2dtc)_2$ (29 mg, 0.07 mmol), and an excess of HMTA (40 mg, 0.28 mmol) were dissolved in 16 mL of chlorobenzene/benzonitrile solution (15:1) by stirring for 4 h at 60 °C. The solution was cooled down and filtered. The evaporation of the solution during one week afforded the crystals of **11**. The crystals were filtered off and washed with several portions of acetone to give black prisms with 80% yield.

The crystals of $\{Hg(Et_2dtc)_2\}_2\cdot C_{60}$ (**12**) were obtained similarly to **3**–**6**. However, according to X-ray diffraction data complex **12** crystallizes without inclusion of DABCO. $Hg(CH_3COO)_2\cdot 4H_2O$ (0.087 mmol), two molar equivalents of $Na(Et_2dtc)$ (0.26 mmol), and an excess of DABCO (100 mg, 0.9 mmol) were stirred in dichlorobenzene (12 mL) for 4 h at 60 °C. The solution was cooled down and filtered, and C_{60} (25 mg, 0.035 mmol) was dissolved during 2 h at 60 °C. The solution was cooled down again and filtered into the tube for the diffusion of 45 mL volume, and 30 mL of hexane was layered over the dichlorobenzene solution. After one month, prisms of **12** grew on the walls of tube.

The compositions of the complexes were determined by elemental (**1**, **4**, **8**, and **10**) and X-ray structural analysis on single crystals (**2**, **3**, **5**, **6**, **7**, **9**, **11**, and **12**) (Table 1). As a rule, several crystals were tested

Table 1. Compositions and Data of Elemental Analysis for 1−12[a]

N	complex	elemental analysis (found/calc)					
		C, %	H, %	N, %	Cl, %	S, %	M, %
1	$[\{Cd(EtMedtc)_2\}_2 \cdot DABCO] \cdot C_{60} \cdot (C_6H_5Cl)_{0.5}$	62.76	2.72	5.55	1.29		
		61.85	2.85	5.09	1.08	15.51	13.62
2	$[\{Zn(Et_2dtc)_2\}_2 \cdot DABCO] \cdot C_{60} \cdot C_6H_5Cl$	according to X-ray structural analysis					
3	$[\{Cd(Et_2dtc)_2\}_2 \cdot DABCO] \cdot C_{60} \cdot (DABCO)_2$	according to X-ray structural analysis					
4	$[\{Zn(Et_2dtc)_2\}_2 \cdot DABCO] \cdot C_{60} \cdot (DABCO)_2$	66.12	3.84	7.97			
		65.95	4.29	7.91		14.46	7.39
5	$[\{Mn(Et_2dtc)_2\}_2 \cdot DABCO] \cdot C_{60} \cdot (DABCO)_2$	according to X-ray structural analysis					
6	$[\{Fe(Et_2dtc)_2\}_2 \cdot DABCO] \cdot C_{60} \cdot (DABCO)_2$	according to X-ray structural analysis					
7	$[\{Cd(iPr_2dtc)_2\}_2 \cdot DABCO] \cdot C_{60} \cdot (C_6H_{14})_{0.88} \cdot (C_6H_4Cl_2)_{0.12}$	according to X-ray structural analysis					
8	$[\{Cd(nPr_2dtc)_2\}_2 \cdot DMP] \cdot (C_{60})_5 \cdot (C_6H_5Cl)_4$	84.85	1.70	1.94	2.56		
		84.38	1.76	1.65	2.78	5.02	4.41
9	$[\{Hg(nPr_2dtc)_2\}_2 \cdot DMP] \cdot (C_{60})_5 \cdot (C_6H_5Cl)_4$	according to X-ray structural analysis					
10	$[\{Zn(nBu_2dtc)_2\}_2 \cdot DMP] \cdot (C_{60})_7 \cdot (C_6H_5Cl)_4$	88.85	2.23	1.17	2.15		
		89.07	1.61	1.27	2.16	3.90	1.99
11	$[\{Zn(Et_2dtc)_2\} \cdot HMTA]_2 \cdot C_{60} \cdot C_6H_5Cl$	according to X-ray structural analysis					
12	$\{Hg(Et_2dtc)_2\}_2 \cdot C_{60}$	according to X-ray structural analysis					

[a] EtMedtc: ethylmethyldithiocarbamate; Et_2dtc: diethyldithiocarbamate; iPr_2dtc: di(*i*-propyl)dithiocarbamate; nPr_2dtc: di(*n*-propyl)dithiocarbamate; nBu_2dtc: di(*n*-butyl)dithiocarbamate.

from each synthesis by X-ray structural analysis, and it was shown that they have the same unit cell parameters.

General. UV–visible−NIR spectra were measured on a Shimadzu-3100 spectrometer in the 240–2600 nm range. FT-IR spectra were measured in KBr pellets with a Perkin-Elmer 1000 Series spectrometer (400–7800 cm^{-1}). A Quantum Design MPMS-XL SQUID magnetometer was used to measure static magnetic susceptibilities of **5** and **6** from 1.9 up to 300 K in a 100 mT static magnetic field. A sample holder contribution and core temperature independent diamagnetic susceptibility (χ_0) were subtracted from the experimental values. The values of Θ and χ_0 were calculated in the 50–300 K range by fitting experimental data using the appropriate formula: $\chi_M = C/(T - \Theta) + \chi_0$. The EPR spectra were recorded for **5** and **6** from 4 K up to room temperature (RT = 293 K) with a JEOL JES-TE 200 X-band ESR spectrometer equipped with a JEOL ES-CT470 cryostat. The EPR measurements in Lausanne were performed with a Bruker ELEXYS E500 spectrometer equipped with an Oxford ESR900 cryostat. The photoconductivity spectra were recorded using the light of a xenon lamp transmitted through the monochromator. To study magnetic field effects on photoconductivity, the complexes were excited by white light of a halogen tube. Light intensity was $10^{12}-10^{14}$ photons/cm^2 s. A measuring cell containing a single crystal sample in a quartz ampule was placed into the cavity of a standard RadioPan SE/X 2547 ESR spectrometer. Silver contacts attached to one of the surfaces of the sample were under direct voltage of 10–50 V. Current values were measured with an electrometric amplifier. All photoconductivity measurements were carried out at RT.

X-ray Crystal Structure Determination. X-ray diffraction data for **2**, **3**, and **6** were collected at 90(2) K using a Bruker SMART1000 CCD diffractometer installed at a rotating anode source (Mo Kα radiation, $\lambda = 0.71073$ Å) and equipped with an Oxford Cryosystems nitrogen gas-flow apparatus. The data were collected by the rotation method with 0.3° frame-width (ω scan) and 10 s exposure time per frame. Four sets of data (600 frames in each set) were collected, nominally covering half of the reciprocal space. The data were integrated, scaled, sorted, and averaged using the SMART software package.[15] The structures were solved by the direct methods using SHELXTL NT Version 5.10.[15] X-ray diffraction data for **5**, **7**, **9**, **11**, and **12** were collected at 95–100(2) K using a Bruker Nonius X8 Apex diffractometer with a CCD area detector (Mo Kα radiation, $\lambda = 0.71073$ Å) equipped with an Oxford Cryosystems nitrogen gas-flow apparatus. The data were collected by φ- and ω-scans with 0.3° frame-width and 30 s exposure time per frame. The data were integrated, scaled, sorted, and averaged using the Bruker AXS software package.[16] The structure was solved by the direct methods using SHELXTL Version 6.12.[16] The structures were refined by full-matrix least-squares against F^2. Non-hydrogen atoms were refined in the anisotropic approximation. Positions of hydrogen atoms were calculated geometrically. Subsequently, the positions of H atoms were refined by the "riding" model with $U_{iso} = 1.2U_{eq}$ of the connected non-hydrogen atom or as ideal CH_3 groups with $U_{iso} = 1.5U_{eq}$. The details of X-ray crystal structure analysis for **2**, **3**, **5**, **6**, **7**, **9**, **11**, and **12** including CCDC numbers for the structures are given in Table 2.

Unit cell parameters for **8** were determined by X-ray diffraction experiments on a single crystal.

Disorder in the Complexes. C_{60} and metal(II) dithiocarbamate molecules are ordered in **2**, **3**, **5**, **6**, **11**, and **12**. In **7** C_{60} molecules are disordered between two orientations with the 0.75/0.25 occupancies. One of three crystallographically independent C_{60} molecules in **9** is statistically disordered between two orientations linked by the rotation about the axis passing through the centers of two oppositely located C_{60} hexagons. DABCO is statistically disordered in **2**, **3**, **5**, **6**, and **7** between two orientations linked by the rotation of the molecule by 60° about the axis passing through two nitrogen atoms of DABCO. C_6H_5Cl molecules are statistically disordered between two orientations in **2**. The position of solvent molecules in **7** is shared by hexane (two orientations with the 0.44 occupancies) and $C_6H_4Cl_2$ (two orientations with the 0.08 occupancies). There are two positions of C_6H_5Cl molecules in **9**. In one position, C_6H_5Cl molecules are disordered between two orientations with the 0.92/0.08 occupancies, and in the second position they are disordered between three positions with the 0.67/0.18/0.15 occupancies. In **11**, C_6H_5Cl molecules are disordered between four positions with the 0.42/0.34/0.09/0.09 occupancies.

Results and Discussion

1. Synthesis. Complexes **1–12** were obtained by the evaporation and diffusion techniques, and their compositions were determined from elemental analysis and from X-ray diffraction data on single crystals (Table 1). In the design of these complexes, we used self-assembly of metal(II) dithiocarbamates with bi- and tetradentant nitrogen-containing ligands, which results in new supramolecular assemblies able to cocrystallize with fullerenes. C_{60} complexes containing $\{M^{II}(R_2dtc)_2\}_2 \cdot$ DABCO dimers can be obtained only for R = Et, Me; Et, and *i*Pr. Probably, the length of substituents (R) is defined by packing factors, and dimers of metal(II) dithiocarbamates with short (R = Me) or longer (R = *n*Pr) alkyl substituents do not form complexes with C_{60}. The range of metals, which can be used in these coordination assemblies, is limited by M = Zn, Cd, Fe^{II}, and Mn^{II}. In the same conditions, $Hg^{II}(Et_2dtc)_2$ forms complex **12** without inclusion of DABCO. $M^{II}(R_2dtc)_2$, which reduce C_{60} in solution (M = V^{II} and Co^{II}),[7b] do not form crystalline complexes. $\{M^{II}(R_2dtc)_2\}_2 \cdot DMP$ dimers (M = Zn, Cd, and Hg) form complexes with C_{60} only with longer alkyl substituents (R = *n*Pr and *n*Bu).

2. Crystal Structures of the Complexes. 2.1. Molecular Structures of the Metal(II) Dithiocarbamate Dimers and Monomers. The bond lengths and angles for the coordination

Table 2. Crystallographic Data[a]

compound	**2**	**3**	**5**	**6**	**7**	**9**	**11**	**12**
structural formula	$[\{Zn(Et_2dtc)_2\}_2\cdot DABCO]\cdot C_{60}\cdot C_6H_5Cl$	$[\{Cd(Et_2dtc)_2\}_2\cdot DABCO]\cdot C_{60}\cdot (DABCO)_2$	$[\{Mn(Et_2dtc)_2\}_2\cdot DABCO]\cdot C_{60}\cdot (DABCO)_2$	$[\{Fe(Et_2dtc)_2\}_2\cdot DABCO]\cdot C_{60}\cdot (DABCO)_2$	$[\{Cd(iPr_2dtc)_2\}_2\cdot DABCO]\cdot C_{60}\cdot (C_6H_4Cl_2)_{0.12}\cdot (C_6H_{14})_{0.88}$	$[\{Hg(nPr_2dtc)_2\}_2\cdot DMP]\cdot (C_{60})_5\cdot (C_6H_5Cl)_4$	$[\{Zn(Et_2dtc)_2\}\cdot HMTA]_2\cdot C_{60}\cdot C_6H_5Cl$	$[\{Hg(Et_2dtc)_2\}_2\cdot C_{60}$
empirical formula	$C_{92}H_{57}ClN_6S_8Zn_2$	$C_{98}H_{76}N_{10}S_8Cd_2$	$C_{98}H_{76}N_{10}S_8Mn_2$	$C_{98}H_{76}N_{10}S_8Fe_2$	$C_{100}H_{80.80}Cl_{0.24}\ N_6S_8Cd_2$	$C_{358}H_{90}Cl_4N_6S_8Hg_2$	$C_{98}H_{69}ClN_{12}S_8Zn_2$	$C_{80}H_{40}N_4S_8Hg_2$
F_w, g mol^{-1}	1669.20	1870.94	1760.05	1757.84	1856.29	5273.82	1837.32	1714.82
color crystal shape	black parallelepiped	black parallelepiped	black parallelepiped	black parallelepiped	black plate	black prism	black prism	black prism
cryst system	orthorhombic	orthorhombic	orthorhombic	orthorhombic	orthorhombic	monoclinic	triclinic	monoclinic
space group	*Pbam*	*Pbam*	*Pbam*	*Pbam*	*Ibam*	$P2_1/n$	$P\bar{1}$	$P2_1/n$
a, (Å)	10.2365(5)	10.4576(3)	10.44310(4)	10.3490(4)	11.7155(3)	16.9422(11)	10.3921(4)	16.1521(5)
b, (Å)	16.8848(8)	17.0583(5)	17.0608(6)	16.9698(7)	16.5374(4)	20.1412(13)	16.9217(6)	16.9573(4)
c, (Å)	20.8180(10)	20.9776(5)	20.9215(7)	20.8387(9)	42.0900(8)	29.786(2)	22.3916(8)	10.5560(3)
α, deg	90	90	90	90	90	90	84.1470(10)	90
β, deg	90	90	90	90	90	94.9170(10)	76.6500(10)	99.7330(10)
γ, deg	90	90	90	90	90	90	89.8850(10)	90
V (Å^3)	3598.2(3)	3742.2(2)	3726.8(2)	3659.7(3)	8154.7(3)	10126.6(11)	3810.3(2)	2849.63(14)
Z	2	2	2	2	4	2	2	2
D_c (g cm^{-3})	1.515	1.660	1.568	1.595	1.512	1.730	1.601	1.999
μ (mm^{-1})	0.992	0.854	0.626	0.689	0.790	1.731	0.948	5.733
T (K)	90(3)	90(1)	100(2)	90(1)	100(2)	100(2)	95(2)	100(2)
max 2θ, deg	54.04	77.46	56.56	68.65	54.96	56.5	54.2	56.56
absorp cor	SADABS	SADABS	SADABS	SADABS	SADABS	SADABS	SADABS	SADABS
reflns meas	47259	165581	24899	73217	30288	52049	24119	23241
unique reflns (R_{int})	4048 (0.046)	10623 (0.0236)	4708 (0.0165)	7539 (0.022)	4704 (0.0230)	24480 (0.0200)	16328 (0.0143)	6956 (0.0204)
parameters restraints	247 25	292 0	305 3	292 0	442 373	1776 1825	1153 115	429 0
reflns, $F > 2\sigma(F)$	3367	9580	4415	6663	4126	21358	14634	6294
R_1 $[F > 2\sigma(F)]$	0.0548	0.0237	0.0364	0.0342	0.0252	0.0561	0.0376	0.0218
wR_2	0.1580	0.0649	0.1130	0.1499	0.0618	0.1501	0.0885	0.0623
GOF	1.137	1.036	1.067	1.365	1.054	1.047	1.050	1.169
CCDC	614488	614489	638245	614490	638242	638244	638246	638243

[a] Crystallographic data for **8**: monoclinic, space group $P2_1/n$, $a = 17.0722(7)$, $b = 20.0758(7)$, $c = 29.6701(12)$ Å, $\beta = 94.965(1)°$, $V = 10131.1(11)$ Å^3, $z = 2$, $T = 100(2)$ K.

Table 3. Geometric Parameters for Metal(II) Dialkyldithiocarbamates, Their Coordination Assemblies, and Donor−Fullerene Interaction in the Complexes

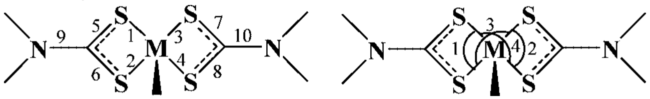

complex:	**2**	**3**	**5**	**6**	**7**	**9**	**11**		**12**
							monomer, Zn, HMTA		
unit, metal and ligand:	dimer, Zn, DABCO	dimer, Cd, DABCO	dimer, Mn, DABCO	dimer, Fe, DABCO	dimer, Cd, DABCO	dimer, Hg, DMP	1	2[b]	dimer, Hg
bond length, Å:									
1	2.5909(10)	2.7050(2)	2.4872(4)	2.5241(3)	2.6011(4)	2.7300(11)	2.6254(6)	2.6414(6)	2.5046(7)
2	2.3459(8)	2.5438(2)	2.5971(5)	2.4024(3)	2.5907(4)	2.5411(10)	2.3533(6)	2.3446(6)	2.6259(7)
3	2.3460(8)	2.5438(2)	2.5971(5)	2.4024(3)	2.5907(4)	2.9420(11)	2.3543(6)	2.3557(6)	2.4629(7)
4	2.5909(10)	2.7050(2)	2.4872(4)	2.5241(3)	2.6011(4)	2.4207(10)	2.5802(6)	2.5714(6)	3.1672(8)
5	1.716(3)	1.7204(8)	1.7309(18)	1.7192(12)	1.7295(18)	1.716(4)	1.719(2)	1.718(2)	1.733(3)
6	1.724(4)	1.7326(8)	1.7250(17)	1.7250(12)	1.7335(17)	1.730(4)	1.737(2)	1.733(2)	1.736(3)
7	1.724(4)	1.7326(8)	1.7250(17)	1.7250(12)	1.7335(17)	1.682(4)	1.727(2)	1.736(2)	1.716(3)
8	1.716(3)	1.7204(8)	1.7309(18)	1.7192(12)	1.7295(18)	1.748(4)	1.724(2)	1.724(2)	1.738(3)
9	1.326(5)	1.3343(10)	1.332(2)	1.3337(14)	1.336(2)	1.344(5)	1.329(3)	1.330(3)	1.325(4)
10	1.326(5)	1.3343(10)	1.332(2)	1.3337(14)	1.336(2)	1.341(5)	1.331(3)	1.325(3)	1.331(4)
M•••S (**1**–**4**) aver	2.468	2.623	2.5422	2.463	2.5959	2.658	2.478	2.478	2.5548
bond angles, °									
1	72.86(3)	69.064(6)	71.155(13)	72.601(10)	69.426(13)	68.99(3)	72.325(2)	72.269(2)	69.73(2)
2	72.86(3)	69.064(6)	71.155(13)	72.601(10)	69.426(13)	66.52(3)	73.220(2)	73.319(2)	63.14(2)
3	145.75(5)	150.702(10)	148.32(3)	146.507(18)	157.31(2)	141.14(4)	145.68(2)	144.40(2)	143.41(2)
4	159.48(5)	163.779(11)	161.23(3)	159.740(19)	162.50(2)	158.01(3)	160.92(2)	161.16(2)	156.27(2)
dihedral angle between NCS$_2$M planes	143.93	148.94	146.45	144.78	154.65	137.84	145.37	144.05	144.37
N(ligand)•••M, Å	2.138(5)	2.3419(11)	2.241(2)	2.1655(16)	2.362(2)	2.508(4)	2.121(2)	2.123(2)	S•••M (axial) 2.6259(7)
M•••M dist, Å	6.877	7.259	7.077	6.922	7.322	6.530			3.939
M•••C(ful), Å	3.568, 3.568	3.461, 3.461	3.520, 3.520	3.560, 3.560	3.460, 3.460	4.061, 4.320	3.534	3.557	3.569, 3.615
S•••C(ful), Å	3.62–3.71	3.60–3.75	3.59–3.80	3.61–3.83	3.55–3.94	3.443–3.448	3.566–3.581		3.497–3.698
N•••C(ful), Å	3.67–3.69	3.63–3.71	3.583	3.56–3.63	3.77	3.243–3.707	3.332–3.265		3.75
H•••C(ful), Å	2.89–3.01	2.87–3.02	2.826	2.82–3.06	>3.4	>3.30	2.840–2.894		2.891
dihedral angles between NCS$_2$M and C$_{60}$ hexagon planes	4.76, 4.76	5.70, 5.70	5.00, 5.00	4.56, 4.56	16.76, 16.76	19.43 (only one hexagon)	5.03 4.21	5.32 2.62	0.98, 10.19
packing of fullerenes (see Scheme 2)	square layers, 4 neigh	square layers, 4 neigh	square layers, 4 neigh	square layers, 4 neigh	layers, isolated	3D, 6–7 neigh[a]	square layers, 4 neigh		square layers, 4 neigh
interfullerene center-to-center distances, Å	9.873(×4) 10.237(×2)	10.004(×6) 10.458(×2)	10.001(×4) 10.441(×2)	9.938(×4) 10.349(×2)	10.113(×4) 11.716(×2)	9.714–10.281	9.920(×2) 10.392(×2)	9.938(×2)	9.987(×4) 10.556(×2)
interfullerene C•••C contacts, Å (<3.45 Å)	3.325–3.372	3.367	3.369	3.311–3.399	>3.57	3.078–3.470	3.296–3.385		3.229–3.393

[a] There are three crystallographically independent C$_{60}$ molecules in **9**, two of which have six C$_{60}$ neighbors and one has seven C$_{60}$ neighbors. [b] Data for two crystallographically independent {Zn(Et$_2$dtc)$_2$}•HMTA units.

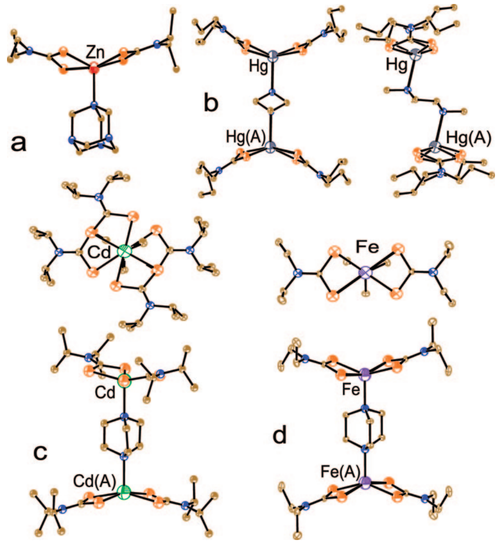

Figure 1. Molecular structures of the coordination assemblies of metal(II) dithiocarbamates in the complexes with C_{60}: (a) $\{Zn(Et_2dtc)_2\}\cdot HMTA$ monomer in **11**; (b) $\{Hg(nPr_2dtc)_2\}_2\cdot DMP$ dimer in **9**; (c) $\{Cd(iPr_2dtc)_2\}_2\cdot DABCO$ dimer in **7**; (d) $\{Fe^{II}(Et_2dtc)_2\}_2\cdot DABCO$ dimer in **6**. $\{M^{II}(Et_2dtc)_2\}_2\cdot DABCO$ (M = Zn, Cd and Mn^{II}) in **2**, **3**, and **5** have similar molecular structures. Carbon atoms are shown in brown, sulfur atoms are in red-orange, and nitrogen atoms are in blue.

assemblies of metal(II) dithiocarbamates in the complexes with C_{60} are listed in Table 3, and their molecular structures are shown in Figure 1. Pristine $Fe^{II}(Et_2dtc)_2$, $Zn(R_2dtc)_2$, $Cd(R_2dtc)_2$, and $Hg^{II}(R_2dtc)_2$ (R = alkyl) form $\{M(R_2dtc)_2\}_2$ dimers through the additional axial coordination of sulfur to the metal atom of the adjacent $M^{II}(R_2dtc)_2$ unit.[17] Metal ions are five coordinated in such dimers. However, their environment is closer to the tetrahedral one since one equatorial M−S bond (2.613, 2.825, 2.800, and 3.127 Å, respectively) is essentially longer than four other M−S bonds (averaged at 2.425, 2.378, 2.580, 2.564 Å, respectively[17]). $Mn^{II}(Et_2dtc)_2$ form polymers with the distorted octahedral environment of Mn^{II} ions.[18] Metal(II) dithiocarbamates can also exist in a monomeric form, for example, planar $Hg^{II}(R_2dtc)_2$[19] or tetrahedral $Zn(R_2dtc)_2$ in the complexes with C_{60}.[7b]

DABCO and DMP are strong bidentant ligands and form coordination dimers namely with metal (II) dithiocarbamates, which trend to fifth extra coordination (Zn, Cd, Hg, Mn, and Fe). The axial M−N(L) bonds in the $\{M^{II}(R_2dtc)_2\}_2\cdot L$ units are noticeably shorter than equatorial M−S(dtc) bonds and increase in the order: Zn (2.14 Å) < Fe (2.16 Å) < Mn (2.24 Å) < Cd (2.34–2.36 Å) < Hg (2.51 Å). Close M−N(L) bonds lengths were found in fullerene free coordination assemblies with $Zn(Et_2dtc)_2$ (2.08–2.14 Å) and $Cd(Et_2dtc)_2$ (2.42 Å).[12a,c] The averaged length of the equatorial M−S(dtc) bonds increases in the complexes in the following order: Fe (2.46 Å) ≤ Zn (2.47 Å) < Mn (2.54 Å) < Cd (2.60–2.62 Å) < Hg (2.66 Å). One can observe obvious tendency to the increase of the lengths of both M−N(L) and M−S(dtc) bonds with the increase of covalent radii of the central metal(II) ion in dithiocarbamate [Zn (0.74 Å), Fe^{II} (0.74 Å), Mn^{II} (0.80 Å), Cd (0.97 Å), Hg^{II} (1.10 Å)[31]].

A comparative analysis of the geometries of $M^{II}(R_2dtc)_2$ in pristine $\{M^{II}(R_2dtc)_2\}_2$ compounds with those in the coordination $\{M^{II}(R_2dtc)_2\}_2\cdot L$ dimers in the complexes with C_{60} shows that in the former case three short and one long equatorial M−S(dtc) bonds are formed, whereas in the latter case there are two short equatorial M−S(dtc) bonds and two other M−S(dtc) bonds are 0.12–0.34 Å longer.

Scheme 2

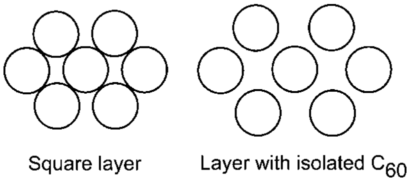

In coordination $\{M^{II}(Et_2dtc)_2\}_2\cdot DABCO$ dimers, two dithiocarbamate units are completely superposed along the axis passing through the metal(II) ions of $M(Et_2dtc)_2$ and nitrogen atoms of DABCO (Figure 1d). On the contrary, in $\{Cd(iPr_2dtc)_2\}_2\cdot DABCO$ (**7**), dithiocarbamate units with bulky *i*Pr substituents rotate relative to each other at an angle of 69.4° (Figure 1c). Though two $Hg(nPr_2dtc)_2$ units do not rotate in the $\{Hg^{II}(nPr_2dtc)_2\}_2\cdot DMP$ dimers (**9**), they are shifted relative to each other by ~2.9 Å. This distance approximately corresponds to the distance between nitrogen atoms in DMP (Figure 1b).

Even though HMTA is a tetradentant ligand, it forms only coordination $\{Zn(Et_2dtc)_2\}\cdot HMTA$ monomers in **11** (Figure 1a). The axial Zn−N(HMTA) bond length (2.12 Å) is the shortest among coordination assemblies studied in this work. There are two short and two longer equatorial Zn−S(dtc) bonds in **11** of nearly the same lengths as those in $\{Zn(Et_2dtc)_2\}_2\cdot DABCO$ (**2**) (Table 3).

2.2. General Features of Metal(II) Dithiocarbamate Dimers and Monomers Packing with C_{60}. C_{60} complexes with $\{M^{II}(Et_2dtc)_2\}_2\cdot DABCO$ dimers (M = Zn (**2**), Cd (**3**), Mn (**5**), and Fe (**6**)) are isostructural. The complex with $\{Cd(iPr_2dtc)_2\}_2\cdot DABCO$ (**7**) has a similar crystal structure. However, the unit cell of **7** is doubled along the *c*-axis. The C_{60} molecules are ordered in the complexes studied due to high steric complementarity between the butterfly-shaped metal(II) dithiocarbamates and nearly spherical C_{60} molecules (Figures 2−6). The exception is **7**, in which the C_{60} molecules are disordered between two orientations, and **9**, in which one of three crystallographically independent C_{60} molecules is disordered.

The butterfly-like shapes of $\{M(R_2dtc)_2\}_2\cdot DABCO$ dimers (Figures 2 and 3) or $\{Zn(Et_2dtc)_2\}\cdot HMTA$ monomers (Figure 4) provide a layered packing of fullerene molecules in the crystals. Complexes **2**, **3**, **5**, **6**, and **11** have a square arrangement of fullerenes in layers with four neighbors for each C_{60} and the shortest center-to-center interfullerene distances of 9.87 (**2**), 9.92–9.94 (**11**), 9.94 (**6**), 10.001 Å (**5**) and 10.004 Å (**3**). Similar center-to-center interfullerene distances in pure C_{60} are 9.94 Å at 153 K.[20] As a result of dense packing, multiple van der Waals (vdW) interfullerene C···C contacts are formed in the layers of **2**, **3**, **5**, **6**, and **11** in the 3.296–3.385 Å range (Table 3). It is seen an obvious tendency for the increase of the center-to-center distances between fullerenes at the increase of the length of M−S bonds in the following order: Zn < Fe < Mn < Cd. Thus, even for isostructural complexes, the variation of metal(II) ions in dithiocarbamates allows one to affect the interfullerene center-to-center distances. Square layers were found in **7** (Figure 3). However, bulkier *i*Pr substituents of $\{Cd(iPr_2dtc)_2\}_2\cdot DABCO$ isolate fullerene molecules from each other because their methyl groups protrude into fullerene layers (Figure 3), whereas in the complexes with densely packed fullerene layers (**2**, **5**, **6**, and **11**) only two of four methyl groups of Et substituents in $M(Et_2dtc)_2$ protrude into these layers (Figure 2). The large interfullerene center-to-center distance of 10.11 Å in **7** prevents

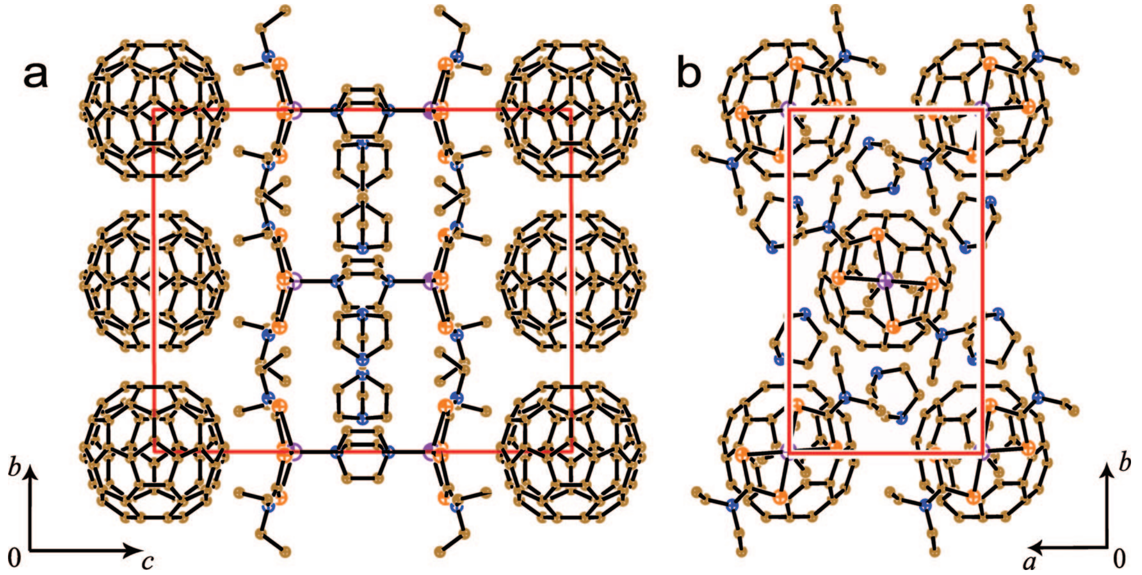

Figure 2. View of crystal structure of **6** along the *a*- (a) and *c*-axes (b). Only one orientation of DABCO is shown.

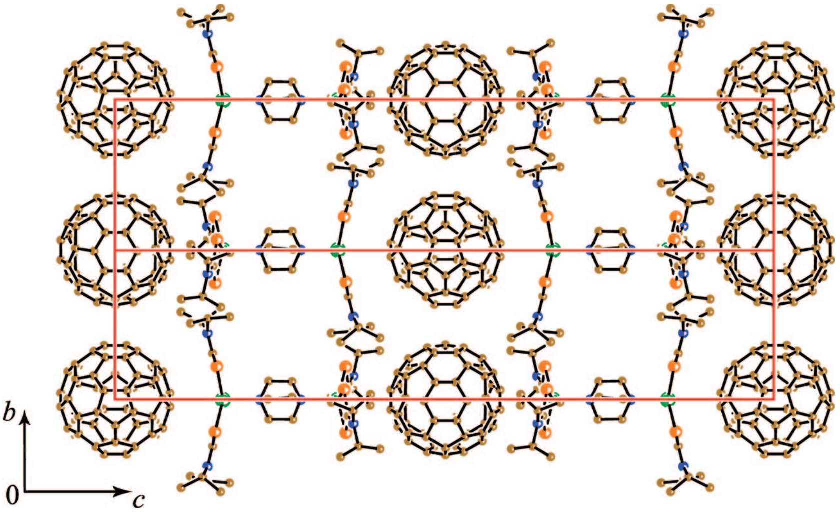

Figure 3. View of the crystal structure of **7** parallel to the diagonal to the *ab* plane. Only one major occupied orientation of disordered C_{60} molecules and one orientation of DABCO are shown. Disordered solvent molecules are omitted for clarity.

the formation of any shortened interfullerene C•••C contacts (all such contacts are longer than 3.45 Å).

The projection of the $\{Fe^{II}(Et_2dtc)_2\}_2$•DABCO layer on the C_{60} one in **6** is shown in Figure 2b. The central part of the FeS_4 fragment is arranged strictly above the C_{60} sphere. The Fe^{II} ion locates close to the middle of the 6–6 bond of C_{60} to allow the formation of the Fe•••C(C_{60}) contacts of 3.56 Å. A similar arrangement of metal(II) dithiocarbamate fragments and C_{60} molecules was found in other layered complexes **2**, **3**, **5**, **7**, and **11** (Figures 3 and 4). The lengths of M•••C(C_{60}) contacts are 3.57 Å in **2**, 3.46 Å in **3** and **7**, 3.52 Å in **5**, and 3.53–3.58 Å in **11**. The observed M•••C(C_{60}) distances are relatively long as compared with those in $\{Cu^{II}(Et_2dtc)_2\}_2$•C_{60} (3.33–3.38 Å),[7a,b] metalloporphyrin−fullerene complexes (2.67–3.10 Å),[6] and C_{60} complexes with coordination $(ZnTPP)_x$•L assemblies (3.10–3.31 Å, $x = 1, 2,$ and 4).[10] The packing of $Fe^{II}(Et_2dtc)_2$ units in the donor layers of **6** has a parquet-like motif (Figure 2b). The same packing motif was found in other layered complexes.

There is free space between the planes of two metal(II) dithiocarbamate units in the $\{M^{II}(R_2dtc)_2\}_2$•DABCO dimers, which is occupied by solvent chlorobenzene molecules in **2** (Table 1). It is interesting that the synthesis of complexes in dichlorobenzene results in the incorporation of two noncoordinated DABCO molecules in **3–6** instead of solvent dichlorobenzene molecules (Table 1). This provides more ordered structures of **3**, **5**, and **6** in comparison with **2**. In **7** free space between the Cd(*i*Pr_2dtc)$_2$ planes is occupied by disordered solvent molecules (hexane and $C_6H_4Cl_2$) used in the synthesis.

{Hg(*n*Pr_2dtc)$_2$}$_2$•DMP dimers form a complex with C_{60} of an unusual composition and fullerene molecules packing (**9**). Complex **8** with the similar {Cd(*n*Pr_2dtc)$_2$}$_2$•DMP dimer is isostructural to **9** (Table 2). Most probably, long *n*Pr substituents do not allow the formation of closely packed fullerene layers, which are observed in **3**, **5**, **6**, **7**, and **11**, and in this case 3D packing of fullerene molecules with large cavities occupied by one {Hg(*n*Pr_2dtc)$_2$}$_2$•DMP dimer and four solvent C_6H_5Cl molecules is observed (Figure 5a,b shows only two of four C_6H_5Cl molecules in the cavity). **8** and **9** have a fullerene-reach composition with a 1:5 ratio between the {M(*n*Pr_2dtc)$_2$}$_2$•DMP dimers and C_{60}. For better understanding, 3D packing of **9** can be divided into two types of layers alternating along the

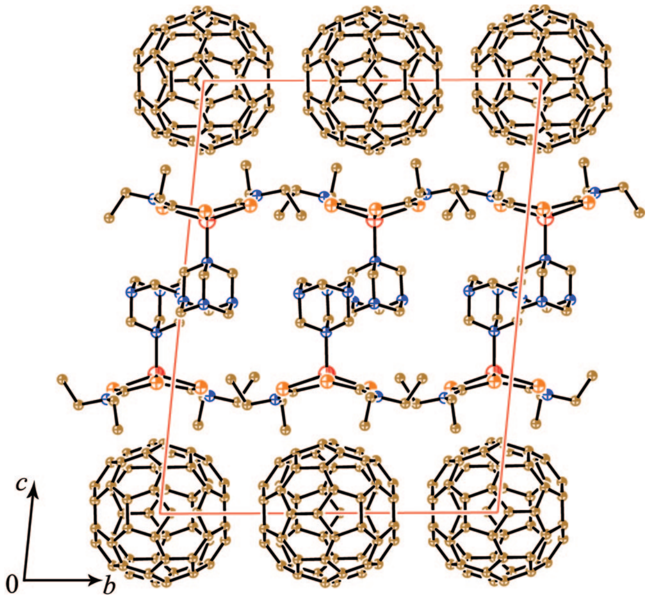

Figure 4. View of crystal structure of **11** along the *a*-axis. Disordered C_6H_5Cl molecules are omitted for clarity.

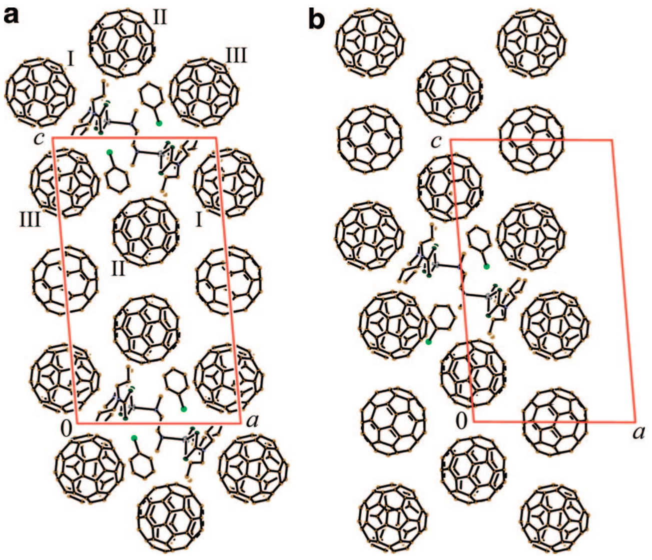

Figure 5. View of crystal structure of **9** along the *b*-axis. The 3D structure of **9** can be presented by two types of layers alternating along the *b*-axis (shown in panels *a* and *b*). Only one orientation of C_{60} molecule of type III and one most occupied orientation of disordered C_6H_5Cl molecules are shown.

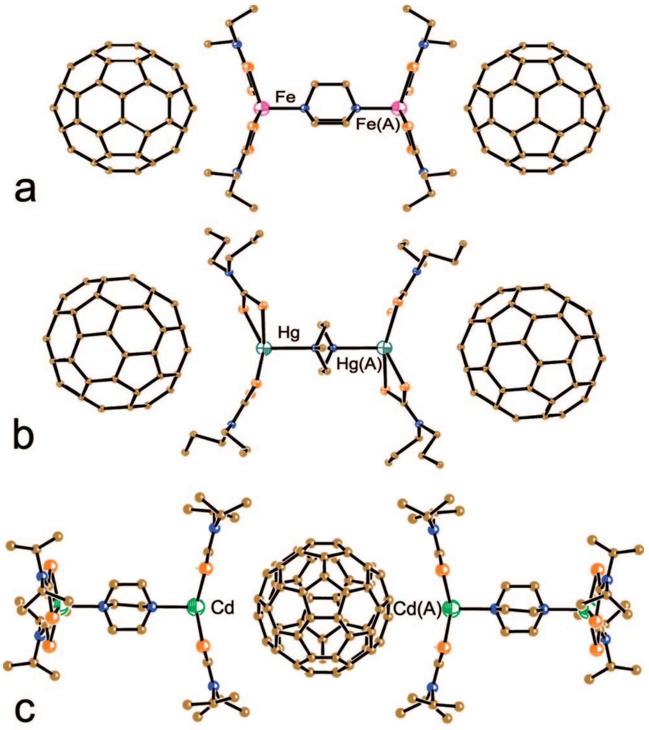

Figure 6. Mutual arrangement of the $\{Fe^{II}(Et_2dtc)_2\}_2 \cdot$DABCO dimer and C_{60} molecules in **6** (a); the $\{Hg^{II}(nPr_2dtc)_2\}_2 \cdot$DMP dimer and C_{60} molecules in **9** (b); and $\{Cd(iPr_2dtc)_2\}_2 \cdot$DABCO dimers and C_{60} molecule in **7** (only one orientation of C_{60} is shown) (c).

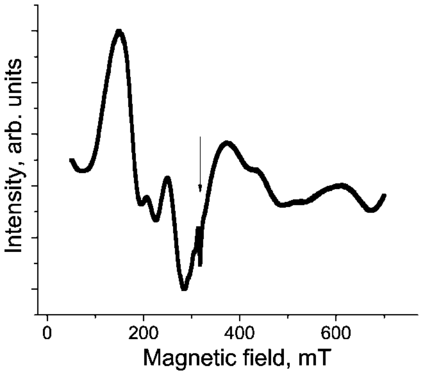

Figure 7. EPR spectrum of polycrystalline $[\{Mn^{II}(Et_2dtc)_2\}_2 \cdot$DABCO$] \cdot C_{60} \cdot (DABCO)_2$ (**5**) at 5 K (9.405288 GHz frequency). Arrow shows the position of the narrow line, which can be attributed to the reduction of $C_{120}O$ impurity[22a] or some impurities in starting C_{60}.[22b]

b-direction, which have different positions of the cavity (Figure 5a,b). There are three crystallographically independent C_{60} molecules in **9**, which have a different arrangement relative to the $\{Hg(nPr_2dtc)_2\}_2 \cdot$DMP dimers. C_{60} molecules of the first type are arranged under and below the dimer (similarly to **2**, **3**, **5**, **6**, and **7**) with the vdW N···C(C_{60}) contacts of 3.243–3.707 Å (denoted as I in Figure 5a; these fullerenes are also shown in Figure 6b). C_{60} molecules of the second type (denoted as II in Figure 5a) are arranged between *n*Pr substituents of $Hg(nPr_2dtc)_2$ and form vdW S···C(C_{60}) contacts in the 3.443–3.448 Å range. C_{60} molecules of the third type (denoted as III in Figure 5a) do not form any shortened vdW contacts with the dimers and are disordered. However, these molecules form vdW C and Cl···C(C_{60}) contacts of 3.22–3.28 Å with C_6H_5Cl molecules. Each C_{60} molecule has from six to seven fullerene neighbors with multiple interfullerene vdW C···C contacts in the 3.078–3.470 Å range. The $\{Hg(nPr_2dtc)_2\}_2 \cdot$DMP dimers are isolated from each other. Hg^{II} ions locate close to the middle of the 6–6 bond of C_{60} with the Hg···C(C_{60}) contacts in the 4.06–4.32 Å range (noticeably longer than such contacts in the layered complexes).

Though complex **12** was characterized,[7b] its crystal structure has not been solved so far. Here we for the first time present its crystal structure, which is similar to that of $\{Cd(Et_2dtc)_2\}_2 \cdot C_{60}$.[7b] C_{60} molecules in **12** are closely packed in square layers with 9.987 Å interfullerene center-to-center distances. Geometric parameters for the $\{Hg(Et_2dtc)_2\}_2$ dimers and donor−fullerene interaction are listed in Table 3.

2.3. Peculiarities of the Metal Dithiocarbamate–Fullerene $\pi-\pi$ Interaction. As was shown,[7b] the dihedral angle of 143.8° between two NCS_2Cd planes in $\{Cd(Et_2dtc)_2\}_2$ is close to the

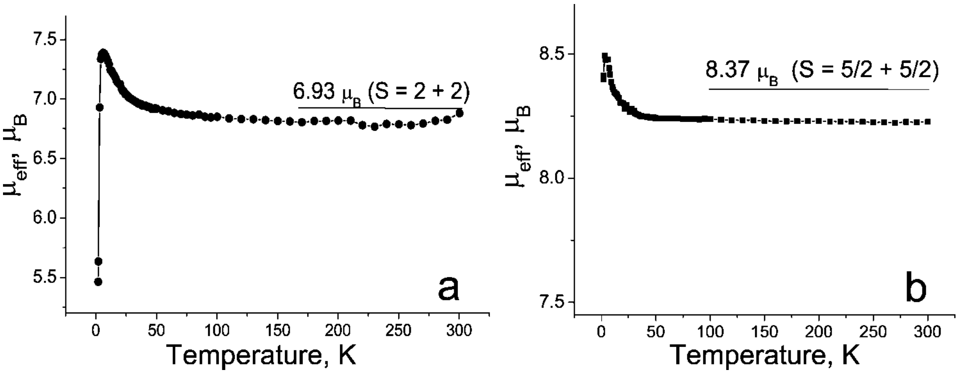

Figure 8. Temperature dependences of magnetic moments of polycrystalline: (a) $[\{Fe^{II}(Et_2dtc)_2\}_2 \cdot DABCO] \cdot C_{60} \cdot (DABCO)_2$ (**6**); (b) $[\{Mn^{II}(Et_2dtc)_2\}_2 \cdot DABCO] \cdot C_{60} \cdot (DABCO)_2$ (**5**) in the 300–1.9 K range. Magnetic moments were calculated per formula unit, which contains two M^{II} centers.

dihedral angle of 138.5° between two C_{60} hexagons. That provides an effective $\pi-\pi$ interaction between dithiocarbamate and fullerene molecules in the complex and, as a result, the dihedral angles between the NCS_2Cd planes and the C_{60} hexagons in $\{Cd(Et_2dtc)_2\}_2 \cdot C_{60}$ are rather small (0 and 8.2°). Because of good sterical compatibility with the shape of the C_{60} molecule, $\{Cd(Et_2dtc)_2\}_2$ nearly quantitatively precipitates complexes with C_{60} from different solvents. Moreover, this complex manifests a relatively intense charge transfer (CT) band in the visible−NIR range.[7b] $\{Cu(Et_2dtc)_2\}_2$ with a more planar $(NCS_2)_2Cu$ fragment (a dihedral angle between two NCS_2Cu planes is 160.9°) shows worse conditions for the $\pi-\pi$ interaction with C_{60}. In this case $\{Cu(Et_2dtc)_2\}_2 \cdot C_{60}$ neither precipitates from solution nor manifests a CT band.[7b] $\{Hg(Et_2dtc)_2\}_2$ in **12** has a dimeric structure (similar to that of $\{Cd(Et_2dtc)_2\}_2$) and rather small dihedral angles between the NCS_2Hg planes and the C_{60} hexagons (1 and 10.2°).

The dihedral angles between two NCS_2M planes in $\{M(R_2dtc)_2\}_2 \cdot DABCO$ (**2**, **3**, **5**, and **6**, Figure 6a) and $\{Zn(Et_2dtc)_2\} \cdot HMTA$ (**12**) are in the range of 144.78–148.94° (Table 3). As a result, the dihedral angles between the NCS_2M planes and the C_{60} hexagons in the complexes are only 4.56–5.70° (Table 3). Smaller (137.8°) dihedral angles as in $\{Hg(nPr_2dtc)_2\}_2 \cdot DMP$ (**9**, Figure 6b) or larger (154.6°) dihedral angles as in $\{Cd(iPr_2dtc)_2\}_2 \cdot DABCO$ (**7**, Figure 6c) between the NCS_2M planes provide the unfavorable conditions for the $\pi-\pi$ interaction with C_{60} (the corresponding dihedral angles are 16.76–19.43°, Table 3). Some disorder of fullerene molecules is observed, namely, in **7** and **9**, whereas C_{60} molecules are ordered in all complexes with effective $\pi-\pi$ interaction.

3. Magnetic Properties of $[\{Mn(Et_2dtc)_2\}_2 \cdot DABCO] \cdot C_{60} \cdot (DABCO)_2$ (5) and $[\{Fe(Et_2dtc)_2\}_2 \cdot DABCO] \cdot C_{60} \cdot (DABCO)_2$ (6). The EPR spectrum of polycrystalline **5** at 5 K is shown in Figure 7. It consists of a complicated signal with several components spread almost over the 0–700 mT range. The main components are centered at 171, 262, 460, and 646 mT (that corresponds to the *g*-factor values of 3.9298, 2.5649, 1.4609, 1.0402, respectively). The appearance of such a spectrum can be explained by a magnetic exchange interaction between two Mn^{II} ions in the $\{Mn(Et_2dtc)_2\}_2 \cdot DABCO$ dimers. Thus, the spectrum of **5** could be more characteristic of binuclear Mn^{II} complexes. Indeed, the spectrum of **5** is similar to those of manganese(II) diethyldithiocarbamate dimers, $\{Mn(Et_2dtc)_2\}_2$, in the complex with C_{70},[7b] binuclear manganese(II) complexes bridged by chlorine atoms,[21a] and coordination $(Mn^{II}TPP)_2 \cdot$ DMP (DMP: *N,N'*-dimethylpiperazine) dimers in the complex with C_{60}.[21b] The absence of the EPR signal, which can be attributed to $C_{60}^{\bullet-}$, indicates the molecular character of **5** with no charge transfer in the ground state. A weak and narrow line at 316 mT (Figure 7, arrow) most probably originates from the reduction of $C_{120}O$ impurity.[22] Though $Mn^{II}(Et_2dtc)_2$ is a strong donor, its redox potential is still more positive than that of C_{60} (the Mn^{3+}/Mn^{2+} transition in $M^{III}(dtc)_3^{1-/0}$ is realized at −0.08 V[23a] vs the first $E^{0/-}$ potential of C_{60} at −0.485 V[23b] (both potentials were measured vs. Ag/AgCl)). Previously, the absence of CT in the ground state was demonstrated for several fullerene complexes with relatively strong Mn^{II} containing donors: manganese (II) diethyldithiocarbamate[7b] and manganese (II) tetraphenylporphyrinate.[6b,d] No EPR signal from $C_{60}^{\bullet-}$ was observed in **6**, and this complex was also attributed to the molecular complexes. $Fe^{II}(Et_2dtc)_2$ is a stronger donor than $Mn^{II}(Et_2dtc)_2$, but its redox potential is still more positive than that of C_{60} (the Fe^{3+}/Fe^{2+} transition in $M^{III}(dtc)_3^{1-/0}$ is realized at −0.37 V vs Ag/AgCl[23a]).

The temperature dependencies of magnetic moments of **5** and **6** are shown in Figure 8a,b. The room-temperature values of magnetic moments of 8.23 and 6.88 μ_B are close to the calculated ones for a system of two noninteracting $S = 5/2$ (8.37 μ_B) and $S = 2$ (6.93 μ_B) spins. Therefore, the Mn^{II} and Fe^{II} ions are in a high-spin state. Magnetic susceptibilities of **5** and **6** follow the Curie–Weiss law in the 50–300 K range with positive Weiss constants of 0.35 and 1.70 K, respectively. Below 35 and 50 K, magnetic moments of **5** and **6** slightly increase in both complexes up to the maximum values of 8.5 μ_B (at 3 K) and 7.4 μ_B (at 6 K) (Figure 8a,b). The increase in the magnetic moments of the complexes together with the positive Weiss constants indicate a weak ferromagnetic interaction between M^{II} spins in the $\{M^{II}(Et_2dtc)_2\}_2 \cdot DABCO$ dimers, which can be mediated by the DABCO ligand. This interaction is a short-range one since coordination dimers are isolated from one another to prevent the formation of a long-range magnetic order. The abrupt decrease of magnetic moments of **5** and **6** observed below 3 and 6 K (Figure 8a,b) can be a result of zero-field splitting of the high-spin anisotropic Mn^{II} and Fe^{II} ions. This effect is small for Mn^{II} containing complex **5** and well-pronounced for Fe^{II} containing complex **6**. Similar magnetic behavior was reported for some hexacyanoferrate and hexacyanochromate $(M^{III}(CN)_6^{3-})$ trinuclear assemblies containing $Mn^{III}(salen)^+$ cations (salen is *N,N'*-ethylenebis(salicylideneaminato) dianion) and its substituted derivatives with high-spin ($S = 2$) Mn^{III} ions.[24] It should be noted that high-spin Fe^{II} in **6** has the same d^4 electronic configuration as Mn^{III}. A more detailed study of the magnetic properties of **5** and **6** is in progress.

The magnetic behavior of **5** containing $\{Mn^{II}(Et_2dtc)_2\}_2\cdot$DABCO is strongly different from that of the C_{70} complex containing$\{Mn^{II}(Et_2dtc)_2\}_2$.[7b] In the latter compound, the Mn^{II} ions also have a high-spin ($S = 5/2$) state. However, the Weiss constant is strongly negative ($\Theta = -96$ K), and magnetic susceptibility decreases even below 46 K because of strong antiferromagnetic interactions between the Mn^{II} ions in $\{Mn^{II}(Et_2dtc)_2\}_2$.[7b] Mn^{II} ions are separated by the DABCO ligand in **5** with a $Mn^{II}\cdots Mn^{II}$ distance of 7.07 Å. As a result, magnetic exchange interaction is weakened due to the increased distance between the adjacent Mn^{II} ions but the character of magnetic interaction between the Mn^{II} ions changes in **5** to a ferromagnetic one.

4. IR- and UV–visible–NIR Spectra of the Complexes. The IR spectra of **1–11** are a superposition of those of starting fullerene, donor, ligand, and solvent molecules (Supporting Information). F_u(1–3) modes of C_{60} at 527, 577, and 1182 cm^{-1}, respectively, retain their position in the spectra of the complexes: 526–527, 575–576, and 1181–1183 cm^{-1}. The band of F_u(4) mode at 1429 cm^{-1} in parent C_{60}, which is most sensitive to charge transfer to the C_{60} molecule,[25] shifts by 1–8 cm^{-1} to smaller wavenumbers in the complexes. Metal(II) dithiocarbamates also have intense bands in the 1427–1435 cm^{-1} range and can contribute to the absorption at 1420–1430 cm^{-1}. In this case, it is impossible to determine the real shift of the F_u(4) mode of C_{60} in the complexes. The formation of coordination units shifts noticeably (by 9–17 cm^{-1}) the position of the intense bands of metal(II) dithiocarbamates in the 1499–1507 cm^{-1} range (Supporting Information) except for **5**.

The UV–visible–NIR spectra of **1–11** are similar (Supporting Information). A typical UV–visible–NIR spectrum of $[\{Fe^{II}(Et_2dtc)_2\}_2\cdot DABCO]\cdot C_{60}\cdot (DABCO)_2$ (**6**) is shown in Figure 9a. The UV-band at 3.67 eV and a weak band at 2.03 eV were attributed to intramolecular transitions in the C_{60} molecules.[26] The band at 2.70 eV can be attributed to the intermolecular CT band between neighboring C_{60} molecules (Figure 9a, CT_1).[27] The observation of this band is possible due to the closely packed arrangement of C_{60} molecules in the complexes. The intensity of this band is weaker in **7** because of quite large distances between C_{60} molecules. This band was not observed in the complexes with isolated C_{60} molecules.[4c,28] Weak and broad absorption in the visible–NIR range with an approximate maximum at about 1.6–1.9 eV can be ascribed to the CT band between $\{Fe^{II}(Et_2dtc)_2\}_2\cdot$DABCO and C_{60} (Figure 9a, CT_2). The bands characteristic of $C_{60}^{\bullet-}$ at 1.33 and 1.18 eV[1b,c] are absent in the spectra of the complexes that is evidence of their neutral ground state.

5. Photoconductivity of the Complexes. Photoconductivity of single crystals of layered $[\{Zn(Et_2dtc)_2\}_2\cdot DABCO]\cdot C_{60}\cdot (DABCO)_2$ (**4**), and complexes with 3D packing of fullerene molecules $[\{Cd(nPr_2dtc)_2\}_2\cdot DMP]\cdot (C_{60})_5\cdot (C_6H_5Cl)_4$ (**8**), and$[\{Hg(nPr_2dtc)_2\}_2\cdot DMP]\cdot (C_{60})_5\cdot (C_6H_5Cl)_4$ (**9**) was studied. Under the illumination of the crystals by white light, the photocurrent increased by 10^2 times in **4** and by 15–20 times in **8** and **9** and then remained unchanged for a long time. This fact proves the absence of any chemical or structural nonequilibrium transformations in the materials.

The photoconductivity spectra for **4**, **8**, and **9** are shown in Figure 9b–d. The spectra manifest maxima at 2.21 and 2.44 eV for **4**, 1.82 eV for **8**, and 1.96 eV for **9**. A comparative analysis of the photoconductivity and absorption spectra shows that the main contribution to the generation of free charge carriers is provided by direct CT from $\{M(R_2dtc)_2\}_2\cdot L$ dimers to C_{60} (the maxima in the absorption spectra at about 1.6–1.9 eV, Figure 9a, CT_2) with a smaller contribution of CT between neighboring C_{60} molecules (the maxima in the absorption spectra at 2.7 eV, Figure 9a, CT_1).

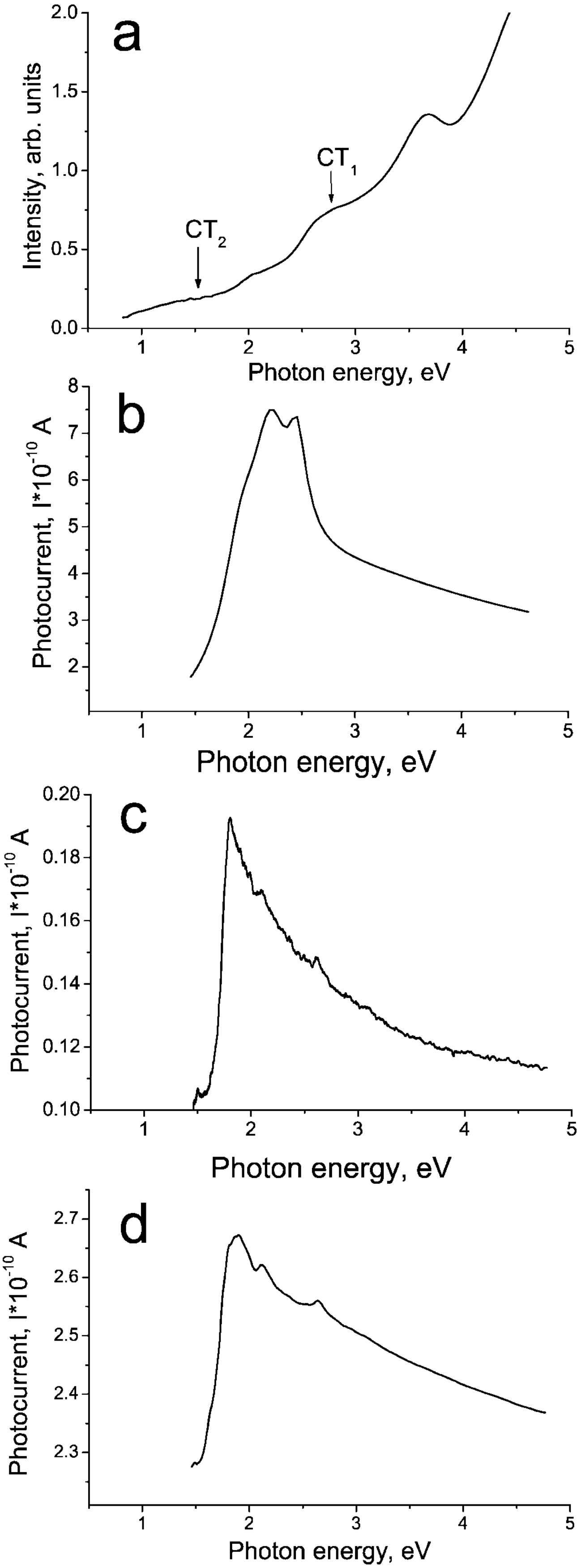

Figure 9. Absorption spectrum of **6** (a) in the 0.5–5 eV range; and the photoconductivity spectra of single crystals of **4** (b); **8** (c); and **9** (d).

Photoexcitation of C_{60} is possible at about 2.03 eV. However, photocurrent strongly decreases at energies higher than 3.5 eV,

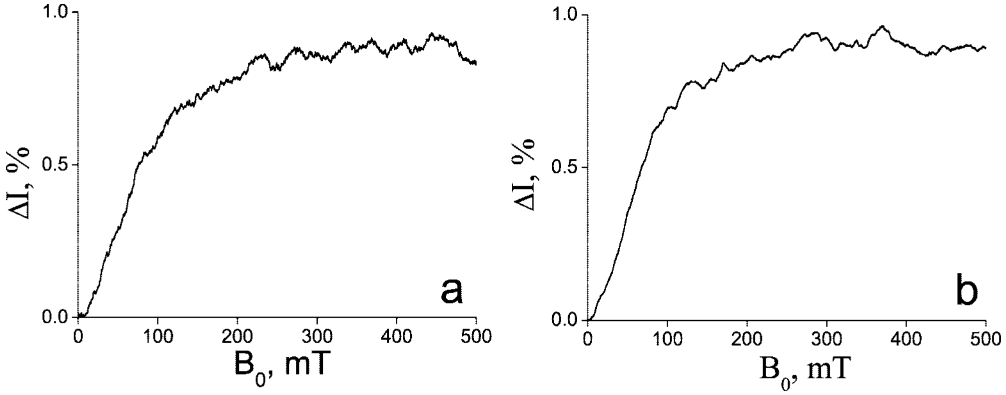

Figure 10. Magnetic field effects on photoconductivity of **8** (a) and **9** (b).

where C_{60} has the strongest absorption. Therefore, the contribution of the C_{60} excitation to the generation of free charge carriers in the complexes is small. Photoexcitation of metal(II) dithiocarbamates does not contribute to the generation of free charge carriers since Zn, Cd, and Hg dithiocarbamates do not absorb in the studied photon energy range.

It was found that white light excited photoconductivity of **8** and **9** increases up to 1% in a weak magnetic field (MF) with induction $B < 1$ T and saturates at $B > 0.2$ T (Figure 10). Positive MF effect on the photoconductivity of the complexes can be described by the following scheme. Light absorption leads to the formation of excitons. They are mainly CT-excitons with electrons and holes localized on the acceptor (C_{60}) and donor ($\{M(R_2dtc)_2\}_2 \cdot L$) molecules, correspondingly. CT-excitons can dissociate on surface, lattice oscillations, defects, and impurities to produce free charge carriers. CT-excitons can be singlet (S) or triplet (T) ones depending on mutual spin orientation. It is known that multiplicity of these intermediate states essentially affects fast processes with the time scale shorter than the spin–lattice relaxation time.[29] Light generates mainly S CT-excitons. Some part of S CT-excitons transfers to T CT-excitons due to the interaction with the lattice and defects. MF also increases the concentration of T CT-excitons due to the S−T intercombination transitions caused by difference of g-factors of ionic states forming CT-excitons. In molecular crystals, the dissociation of intermediate pairs is realized more effectively from T CT-excitons than from S CT-excitons. Since this dissociation produces free charge carriers, photoconductivity increases in MF. Similar positive MF effect on the photocurrent was found in the C_{60} complex with tetrabenzo(1,2-bis[4H-thiopyran-4-ylidene]ethene): $Bz_4BTPE \cdot C_{60}$.[30]

Conclusion

In this work we showed that the supramolecular approach can be successfully applied in the design of new fullerene complexes with metal(II) dithiocarbamate−ligand assemblies. Coordination dimers and monomers formed by $M^{II}(R_2dtc)_2$ (M = Zn, Cd, Hg, Mn, and Fe; R = Me, Et, *i*Pr, *n*Pr, and *n*Bu) with nitrogen-containing ligands (DABCO, DMP, and HMTA) are sterically well consistent with the spherical shape of C_{60} molecules and effectively cocrystallize to form complexes with layered and 3D packing of fullerene molecules (**1**−**11**). The distances between C_{60} molecules in the layers depend on the length of alkyl substituents and the central metal ion of dithiocarbamate. As a result, the packing of C_{60} molecules varies from closely (**2**, **3**, **6**, and **11**) to loosely (**7**) packed square layers. For the first time, we studied the molecular structures of a series of new coordination $\{M^{II}(R_2dtc)_2\}_2 \cdot L$ dimers including those with M = Zn, Cd, Mn, and Fe, R = Et, *i*Pr, L = DABCO (**2**, **3**, **5**, **6**, and **7**); and M = Hg, R = *n*Pr, and L = DMP (**9**). Metal atoms are five-coordinated in the $\{M^{II}(R_2dtc)_2\}_2 \cdot L$ units with one short axial M−N(L) bond and four longer equatorial M−S(dtc) bonds. The length of the axial M−N(L) and equatorial M−S(dtc) bonds increases in the order: Zn = Fe^{II} < Mn^{II} < Cd < Hg^{II} and correlates with the covalent radii of the central metal(II) ions in dithiocarbamate (Zn = Fe^{II} < Mn^{II} < Cd < Hg^{II}).[31] Among equatorial M−S(dtc) bonds, two short and two longer bonds (by 0.12–0.36 Å) can be distinguished, whereas in pristine $\{M^{II}(R_2dtc)_2\}_2$ three of four equatorial M−S(dtc) bonds are short and one bond is essentially longer.[17] Complexes **5** and **6** have magnetic moments of 8.23 and 6.88 μ_B at 300 K, which correspond to the high-spin state of the Mn^{II} ($S = 5/2$) and Fe^{II} ($S = 2$) ions. Magnetic susceptibilities of **5** and **6** follow the Curie–Weiss law in the 50–300 K range with the positive Weiss constants of 0.35 and 1.7 K, respectively. Magnetic moments of the complexes slightly increase below 35 and 50 K, respectively. The positive Weiss constants and the increase of the magnetic moments of the complexes indicate weak ferromagnetic interactions (most probably short-range) between M^{II} spins in the isolated $\{M^{II}(Et_2dtc)_2\}_2 \cdot DABCO$ dimers. Long-range ferromagnetic ordering is not realized in **5** and **6** probably due to relatively long distances between the dimers. The abrupt decrease of the magnetic moments of **5** and **6** below 3 and 6 K is observed and can be associated with zero-field splitting. This effect is more pronounced in **6** containing high-spin Fe^{II} ions with d^4 electronic configuration. On the whole, the experimental data show that in some cases DABCO can efficiently transfer ferromagnetic interaction between metal centers and can be used as a bridging ligand in the design of magnetic assemblies.

Photocurrent increases by 20–100 times in the single crystals of **4**, **8**, and **9** under illumination by white light. The photoconductivity spectra of the complexes have photocurrent maxima at 1.82–2.44 eV. A comparative analysis of the photoconductivity and absorption spectra allows one to conclude that the main contribution to the generation of free charge carriers is provided by direct CT from $\{M^{II}(R_2dtc)_2\}_2 \cdot L$ dimers to C_{60} (the maximum in the absorption spectra at 1.6–1.9 eV), and a smaller contribution is made by intermolecular CT between neighboring C_{60} molecules (the maximum in the absorption spectra at 2.7 eV). It was found that photoconductivity of **8** and **9** is enhanced in a weak magnetic field. It is known that MF increases the concentration of triplet CT-excitons. Since the dissociation of CT-excitons from triplet states occurs more effectively than from singlet ones, the number of free charge carrier increases in MF.

Acknowledgment. The work was supported by the Russian Science Support Foundationan, INTAS YSF 05-109-4653, RFBR Grants N 06-03-32824 and 06-02-96323, and RFBR-JSPS Grant N 06-03-91361, and Grant-in-Aid Scientific Research from the Ministry of Education, Culture, Sports, Science and Technology, Japan (152005019, COE programs). B.N. acknowledges The Swiss National Science Foundation and its NCCR “MaNEP” for financial support.

Supporting Information Available: Crystallographic information files, table of IR spectra data, and UV−visible−NIR spectra. This information is available free of charge via the Internet at http://pubs.acs.org.

References

(1) (a) Balch, A. L.; Olmstead, M. M. *Chem. Rev.* **1998**, *98*, 2123–2165. (b) Konarev, D. V.; Lyubovskaya, R. N. *Russ. Chem. Rev.* **1999**, *68*, 19–38. (c) Reed, C. A.; Bolskar, R. D. *Chem. Rev.* **2000**, *100*, 1075–1120.

(2) (a) Atwood, J. L.; Barbour, L. J.; Raston, C. L.; Sudria, I. B. N. *Angew. Chem., Int. Ed. Engl.* **1998**, *37*, 981–983. (b) Atwood, J. L.; Barbour, L. J.; Nichols, P. J.; Raston, C. L.; Sandoval, C. A. *Chem. Eur. J.* **1999**, *5*, 990–996.

(3) (a) Konarev, D. V.; Zubavichus, Y. V.; Valeev, E. F.; Slovokhotov, Y. L.; Shul′ga, Y. M.; Lyubovskaya, R. N. *Synth. Met.* **1999**, *103*, 2364–2365. (b) Litvinov, A. L.; Konarev, D. V.; Kovalevsky, A. Y.; Neretin, I. S.; Slovokhotov, Y. L.; Coppens, P.; Lyubovskaya, R. N. *CrystEngComm* **2002**, *4*, 618–622.

(4) (a) Izuoka, A.; Tachikawa, T.; Sugawara, T.; Suzuki, Y.; Konno, M.; Saito, Y.; Shinohara, H. *J. Chem. Soc., Chem. Commun.* **1992**, 1472–1473. (b) Saito, G.; Teramoto, T.; Otsuka, A.; Sugita, Y.; Ban, T.; Kusunoki, M.; Sakaguchi, K.-I. *Synth. Met.* **1994**, *64*, 359–368. (c) Konarev, D. V.; Lyubovskaya, R. N.; Drichko, N. V.; Yudanova, E. I.; Shul′ga, Y. M.; Litvinov, A. L.; Semkin, V. N.; Tarasov, B. P. *J. Mater. Chem.* **2000**, 803–818.

(5) Konarev, D. V.; Kovalevsky, A. Y.; Litvinov, A. L.; Drichko, N. V.; Tarasov, B. P.; Coppens, P.; Lyubovskaya, R. N. *J. Solid State Chem.* **2002**, *168*, 474–485.

(6) (a) Olmstead, M. M.; Costa, D. A.; Maitra, K.; Noll, B. C.; Phillips, S. L.; Van Calcar, P. M.; Balch, A. L. *J. Am. Chem. Soc.* **1999**, *121*, 7090–7097. (b) Yudanova, E. I.; Konarev, D. V.; Gumanov, L. L.; Lyubovskaya, R. N. *Russ. Chem. Bull.* **1999**, *48*, 718–721. (c) Boyd, P. D. W.; Hodgson, M. C.; Rickard, C. E. F.; Oliver, A. G.; Chaker, L.; Brothers, P. J.; Bolskar, R. D.; Tham, F. S.; Reed, C. A. *J. Am. Chem. Soc.* **1999**, *121*, 10487–10495. (d) Konarev, D. V.; Neretin, I. S.; Slovokhotov, Y. L.; Yudanova, E. I.; Drichko, N. V.; Shul′ga, Y. M.; Tarasov, B. P.; Gumanov, L. L.; Batsanov, A. S.; Howard, J. A. K.; Lyubovskaya, R. N. *Chem. Eur. J.* **2001**, *7*, 2605–2616.

(7) (a) Konarev, D. V.; Kovalevsky, A. Y.; Lopatin, D. V.; Rodaev, V. V.; Umrikhin, A. V.; Yudanova, E. I.; Coppens, P.; Lyubovskaya, R. N.; Saito, G. *Dalton Trans.* **2005**, 1821–1825. (b) Konarev, D. V.; Kovalevsky, A. Y.; Khasanov, S. S.; Saito, G.; Lopatin, D. V.; Umrikhin, A. V.; Otsuka, A; Lyubovskaya, R. N. *Eur. J. Inorg. Chem.* **2006**, 1881–1895. (c) Konarev, D. V.; Kovalevsky, A. Y.; Otsuka, A.; Saito, G.; Lyubovskaya, R. N. *Inorg. Chem.* **2005**, *44*, 9547–9553.

(8) Atwood, J. L.; Barnes, M. J.; Gardiner, M. G.; Raston, C. L. *J. Chem. Soc. Chem. Commun.* **1996**, 1449–1450.

(9) (a) Konarev, D. V.; Kovalevsky, A. Y.; Coppens, P.; Lyubovskaya, R. N. *Chem. Commun.* **2000**, 2357–2358. (b) Konarev, D. V.; Khasanov, S. S.; Lyubovskaya, R. N.; Otsuka, A.; Saito, G. *Synth. Met.* **2005**, *151*, 231–238. (c) Konarev, D. V.; Kovalevsky, A. Y.; Khasanov, S. S.; Saito, G.; Otsuka, A.; Lyubovskaya, R. N. *Eur. J. Inorg. Chem.* **2005**, 4822–4828.

(10) (a) Konarev, D. V.; Neretin, I. S.; Litvinov, A. L.; Drichko, N. V.; Slovokhotov, Y. L.; Lyubovskaya, R. N.; Howard, J. A. K.; Yufit, D. S. *Cryst. Growth Des.* **2004**, *4*, 643–646. (b) Litvinov, A. L.; Konarev, D. V.; Kovalevsky, A. Y.; Coppens, P.; Lyubovskaya, R. N. *Cryst. Growth Des.* **2005**, *5*, 1807–1819.

(11) (a) Konarev, D. V.; Khasanov, S. S.; Otsuka, A.; Saito, G.; Lyubovskaya, R. N. *Chem. Eur. J.* **2006**, *12*, 5225–5230. (b) Konarev, D. V.; Khasanov, S. S.; Otsuka, A.; Saito, G.; Lyubovskaya, R. N. *J. Am. Chem. Soc.* **2006**, *128*, 9292–9293. (c) Konarev, D. V.; Khasanov, S. S.; Otsuka, A.; Saito, G.; Lyubovskaya, R. N. *Inorg. Chem.* **2007**, *46*, 2261–2271.

(12) (a) Liu, S.-H.; Chem, X.-F.; Zhu, X.-H.; Duan, C.-Y.; You, X.-Z. *J. Coord. Chem.* **2001**, *53*, 223–231. (b) Lai, C. S.; Tiekink, E. R. T. *Appl. Organomet. Chem.* **2003**, *17*, 251–252. (c) Malik, M. M.; Motevalli, M.; O’Brien, P.; Walsh, J. R. *Inorg. Chem.* **1997**, *36*, 1263–1264. (d) Glinskaya, L. A.; Zemskova, S. M.; Klevtsova, R. F.; Larionov, S. V. *Zh. Struct. Khim.* **1996**, *37*, 155–159. (e) Ivanchenko, A. V.; Gromilov, S. A.; Zemskova, S. M.; Baidina, I. A. *Zh. Struct. Khim.* **2000**, *41*, 88–95. (f) Reck, G.; Becker, R. *Acta Crystallogr.* **2004**, *C60*, m134–m136. (g) Zeng, D.; Hampden-Smith, M. J.; Alam, T. M.; Rheingold, A. L. *Polyhedron* **1994**, *13*, 2715–2730.

(13) Rajashree, S.; Krishna Kumar, R.; Udupa, M. R.; Seshasayee, M.; Aravamudan, *Acta Crystallogr.* **1996**, *C52*, 707–709.

(14) Jian, F.; Wang, Z.; Bai, Z.; You, X.; Fun, H.-K.; Chinnakali, K.; Razak, I. A. *Polyhedron* **1999**, *18*, 3401–3406.

(15) (a) *SMART and SAINT, Area Detector Control and Integration Software*, Ver. 6.01; Bruker Analytical X-ray Systems: Madison, WI, 1999. (b) *SHELXTL, An Integrated System for Solving, Refining and Displaying Crystal Structures from Diffraction Data*, Ver. 5.10; Bruker Analytical X-ray Systems: Madison, WI, 1997.

(16) Bruker Analytical X-ray Systems, Madison, WI, USA, 1999.

(17) (a) Ileperuma, D. A.; Feltham, R. D. *Inorg. Chem.* **1975**, *14*, 3042–3045. (b) Bonamico, M.; Mazzone, G.; Vaciago, A.; Zambonelli, L. *Acta Crystallogr.* **1965**, *19*, 898–909. (c) Sreehari, N.; Varghese, B.; Manoharan, P. T. *Inorg. Chem.* **1990**, *29*, 4011–4015. (d) Domenicano, A.; Torelli, L.; Vaciago, A.; Zambonelli, L. *J. Chem. Soc. A* **1968**, 1351–1361. (e) Jian, F.; Wang, Z.; Bai, Z.; You, X.; Fun, H.-K.; Chinnakali, K. *J. Chem. Cryst.* **1999**, *29*, 227–231. (f) Lai, C. S.; Tiekink, E. R. T. *Z. Kristallogr. New Cryst. Struct.* **2002**, *217*, 593–597.

(18) Ciampolini, M.; Mengozzi, C.; Orioli, P. *J. Chem. Soc., Dalton Trans.* **1975**, 2051–2054.

(19) (a) Healy, P. C.; White, A. H. *J. Chem. Soc., Dalton Trans.* **1973**, 284–287. (b) Iwasaki, H. *Acta Crystallogr.* **1973**, *B29*, 2115–2124.

(20) Bürgi, H.-B.; Blanc, E.; Schwarzenbach, D.; Liu, S.; Lu, Y.; Kappes, M. M.; Ibers, J. A. *Angew. Chem., Int. Ed.* **1992**, *31*, 640–643.

(21) (a) Romero, I.; Collomb, M.-N.; Deronyier, A.; Llobet, A.; Perret, E.; Pèkaut, J.; Le Pare, L.; Latour, J.-M. *Eur. J. Inorg. Chem.* **2001**, 69–72. (b) Konarev, D. V.; Khasanov, S. S.; Saito, G.; Otsuka, A.; Lyubovskaya, R. N. *Inorg. Chem.* **2007**, *46*, 7601–7609.

(22) (a) Paul, P.; Kim, K.-C.; Sun, D.; Boyd, P. D. W.; Reed, C. A. *J. Am. Chem. Soc.* **2002**, *124*, 4394–4401. (b) Stankowsky, J.; Byszewsky, P. P.; Kempiński, W.; Trybuła, Z.; Zuk, N. *Phys. Status Solidi B* **1993**, *178*, 221–231.

(23) (a) Van Gaal, H. L. M.; Van der Linden, J. G. M. *Coord. Chem. Rev.* **1982**, *47*, 41–54. (b) Dubois, D.; Kadish, K. M.; Flanagan, S.; Haufler, R. E.; Chibante, L. P. F.; Wilson, L. J. *J. Am. Chem. Soc.* **1991**, *113*, 4364–4366.

(24) (a) Miyasaka, H.; Matsumoto, N.; Re, N.; Gallo, E.; Floriani, C. *Inorg. Chem.* **1997**, *36*, 670–676. (b) Choi, H. J.; Solol, J. J.; Long, J. R. *Inorg. Chem.* **2004**, *43*, 1606–1608. (c) Zhang, J.; Lachgar, A. *J. Am. Chem. Soc.* **2007**, *129*, 250–251.

(25) Picher, T.; Winkler, R.; Kuzmany, H. *Phys. Rev. B* **1994**, *49*, 15879–15889.

(26) Dresselhaus, M. S.; Dresselhaus, G.; Eklund, P. C. *Science of Fullerenes and Carbon Nanotubes*; Academic Press: San Diego, 1996.

(27) Kazaoui, S.; Minami, N.; Tanabe, Y.; Byrne, H. J.; Eilmes, A.; Petelenz, P. *Phys. Rev. B.* **1998**, *58*, 7689–7700.

(28) Konarev, D. V.; Drichko, N. V.; Lyubovskaya, R. N.; Shul `ga, Y. M.; Litvinov, A. L.; Semkin, V. N.; Dubitsky, Yu. A.; Zaopo, A. *J. Mol. Struct.* **2000**, *526*, 25–29.

(29) Buchachenko, A. L.; Frankevich, E. L. *Chemical Generation and Reception of Radio- and Microwaves*; VCH Publishers: New York, 1994; p 180.

(30) Konarev, D. V.; Lopatin, D. V.; Rodaev, V. V.; Umrikhin, A. V.; Khasanov, S. S.; Saito, G.; Nakasuji, K.; Litvinov, A. L.; Lyubovskaya, R. N. *J. Phys. Chem. Solids* **2005**, *66*, 711–715.

(31) Kennard, O. In *CRC Handbook of Chemistry and Physics*; Weast, R. C., Ed.; CRC Press, Inc.: Boca Raton, FL, 1987; p F105.

CG0702481